THE JOURNAL OF PHYSICAL CHEMISTRY C

Article

pubs.acs.org/JPCC

Surface Structure and Electron Transfer Dynamics of the Self-Assembly of Cyanide on Au{111}

Andrew I. Guttentag,[†,‡] Tobias Wächter,[§] Kristopher K. Barr,[†,‡] John M. Abendroth,[†,‡] Tze-Bin Song,[†,∥] Nichole F. Sullivan,[⊥] Yang Yang,[†,∥] David L. Allara,[*,⊥] Michael Zharnikov,[*,§] and Paul S. Weiss[*,†,‡,∥]

[†]California NanoSystems Institute, University of California, Los Angeles, Los Angeles, California 90095, United States

[‡]Department of Chemistry and Biochemistry, University of California, Los Angeles, Los Angeles, California 90095, United States

[§]Applied Physical Chemistry, Heidelberg University, Im Neuenheimer Feld 253, 69120 Heidelberg, Germany

[∥]Department of Materials Science and Engineering, University of California, Los Angeles, Los Angeles, California 90095, United States

[⊥]Department of Chemistry, Pennsylvania State University, University Park, Pennsylvania 16802, United States

Supporting Information

ABSTRACT: A vibronic resonance between Au{111} surface states and adsorbed CN vibrations has been predicted, which we target for study. We have formed stable monolayers of cyanide on Au{111} and observe a hexagonal close-packed lattice with a nearest neighbor distance of 3.8 ± 0.5 Å. Cyanide orients normal to the surface attached via a Au−C bond. We show that the substrate−molecule coupling is particularly strong, leading to ultrafast electron transfer from the cyanide molecules to the Au{111} substrate as measured by resonant Auger spectroscopy using the core−hole clock method. The CN/Au{111} system is a simple example of a strongly interacting adsorbate−substrate system and will be the subject of a number of further studies, as discussed.

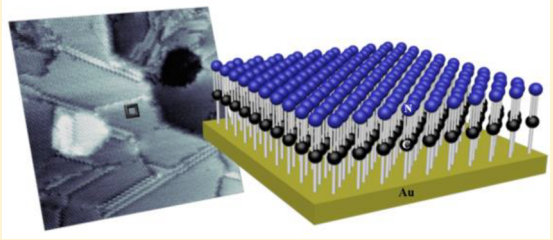

INTRODUCTION

A central theme in nanotechnology is to be able to understand and to manipulate materials at the single-molecule level to advance current technologies and to create new technologies. Self-assembled monolayers (SAMs), in which a single layer of molecules is immobilized on a surface, have often served as platforms for probing the effects of the local environment on molecular structure and function as well as for the development of new materials with distinct physical and chemical properties.[1−8]

Adsorbate−substrate interactions due to immobilization on surfaces strongly influence the function, dynamics, structure, and electronic properties of molecules in SAMs.[9−12] In some cases, as we have demonstrated in our previous work, we can tune the monolayer matrix defect density to affect the function and/or reactivity of molecules that have been tethered to surfaces.[13−18] In other cases, the functional group has been decoupled from the surface through molecular "spacers" to avoid substrate quenching effects from efficient electron transfer.[13,19] Along with affecting electron transport, coupling between the surface electronic structure and molecular vibrations has been observed to enhance the lifetimes and intensities of vibrational modes.[20,21]

Two primary factors, the strength of the electronic coupling between an adsorbed molecule and substrate and the orientation of the molecular orbitals used during transport, directly influence how efficiently an electron is transmitted between molecules to the substrate in SAMs.[22−27] To this end, electron conductance through nitrile-terminated alkanethiol SAMs has been observed to follow an exponential dependence on molecule length with a characteristic decay rate through the application of the core−hole clock (CHC) method in resonant Auger electron spectroscopy (RAES).[25,28,29] These results have shown that inclusion of a four-carbon backbone results in approximately 100× lower efficiency for transferring electrons to the Au{111} substrate with average times of ∼100 fs when compared with the ∼2.5 fs transfer time across only the thiolate headgroup.[30] These data are consistent with other measures of contact conductance.[10,23,24,26,31] The results presented in this work represent the extreme case where the sulfur and carbon backbone are entirely removed and only the nitrile functional group is bound to the Au{111} surface.

Often, the substrate−molecule interface is buried and difficult to probe, requiring special techniques that leverage the well-known chemistry and relatively simple structure of small-molecule probes. One such small molecule is CO, which has been used to elucidate the effect of binding sites on adsorbate vibrational modes.[32] Nevertheless, in the case of CO, as with many small molecules that desorb from surfaces well below room temperature, the ambient environment applica-

Received: June 14, 2016
Revised: October 17, 2016
Published: October 17, 2016

DOI: 10.1021/acs.jpcc.6b06006
J. Phys. Chem. C 2016, 120, 26736−26746

tions are limited. An established coordination chemistry between cyanide and gold[33] has already been leveraged to elucidate the prevalent chemistry, and structure of defects in alkanethiol monolayers,[34,35] to assemble metal−molecule coordination polymers,[36,37] and to probe covalent bond formation between gold atoms,[38] in addition to a component in the fabrication or synthesis of conductive carbon nitride nanomaterials.[39] The coordination complexes formed between cyanide and gold are stable at room temperature. Our previous attempts to assemble CN on Au{111} failed when cyanogen, C_2N_2, did not dissociate under the conditions used.[40] In recent work, we have shown that we can also create monolayers with mixed orientations.[41] Isocyanide[42] and carbene[43] systems have already demonstrated the potential for room temperature self-assembly using Au−C as an alternative to the Au−S bond characterizing thiol systems.

Here, we report the direct observation of the formation of a cyanide SAM on Au{111} under ambient conditions and probe the strength of the Au−CN coupling. Cyanide assembles into a highly ordered, stable, upright monolayer on Au{111} through the formation of a Au−C bond, most likely due to the known gold cyanidation reaction,[44] with a similar surface structure to that observed in SAMs of alkanethiols.[4,5,45] Electron-transfer dynamics are measured by RAES using the core−hole clock method and indicate facile transfer from molecule to the Au{111} substrate. We conclude by discussing electronic, vibration, and structural properties as they relate to substrate−molecule coupling strength and future prospects for the CN/Au{111} system as a platform to study the interactions between molecular vibrations and electronic structure.

EXPERIMENTAL METHODS

Several different Au{111} substrates were used in this study, depending on the specific requirements and parameters of individual experimental techniques. Monolayers of cyanide were prepared in the same fashion for all of these substrates, viz., by placing 0.1 mg of solid KCN (≥96%, Sigma-Aldrich, St. Louis, MO), without any further purification or treatment, in a glass vial with the Au{111} substrate for 24 h at room temperature. ***Caution: KCN is highly toxic and produces the volatile and flammable HCN(g) when it reacts with water and oxygen. It should be used with proper personal protective equipment, in a fume hood, and kept out of extreme temperatures.*** Afterward, the Au{111} substrate was removed from the vial with the KCN and either measured directly or after a short delay or stored under inert gas for delivery to the synchrotrons (see below for details). The monolayers of cyanide were characterized by scanning tunneling microscopy (STM), infrared (IR) spectroscopy, surface-enhanced Raman spectroscopy (SERS), synchrotron-based X-ray photoelectron spectroscopy (XPS), angle-resolved near-edge X-ray absorption fine structure (NEXAFS) spectroscopy, and resonant Auger electron spectroscopy (RAES). Consequently, after the general description of the sample preparation procedure, specific substrates will be described before the description of the particular experiments, viz., STM, IR, SERS, and high-resolution XPS/NEXAFS.

For the STM experiments, Au{111}/mica substrates (150 nm of Au{111}, Agilent Technologies, Santa Clara, CA) were used. The substrates were hydrogen flame annealed, as described previously, to clean the surface and to increase the sizes of the atomically flat terraces.[4,46] After preparation, cyanide monolayers (see above) were allowed to rest in the fume hood for 1 h before being placed in the STM for imaging.

A custom-built, beetle-style STM was used under ambient conditions. All STM images were calibrated against known references: gold step edges for height and a decanethiol on Au{111} SAM matrix for lateral distance measurements. All analyses on STM images were performed using custom software and Matlab.[47,48]

For collecting IR spectra on Au{111}, we used custom-made Au{111}/sapphire prism substrates. Prism substrates were 0.5 cm radius, 1 cm height c-cut sapphire half-cylinders with a 2 nm thick Nb adhesion layer deposited at 0.11 Å/s and a 40 nm thick layer of Au, which is well below the optical penetration depth for metals in the range of the IR frequencies of interest,[49] deposited at a rate of 0.5 Å/s. A bare Au{111}/sapphire prism sample was used for the background spectrum and an incident angle $\theta = 60° > \theta_c = 34.6°$ as measured relative to the surface normal (the critical angle was calculated using $n = 1.76$ and Snell's law, $\theta_c = \sin^{-1}(1/n)$).[49] Infrared spectra were collected using a Thermo-Fisher Nicolet 8700 Interferometer (Thermo-Fisher Scientific, Waltham, MA) and the packaged OMNIC Software (Thermo-Fisher Scientific). The OMNIC software was also used for processing the spectra and identifying peak positions. All samples used for IR measurements were incubated with KCN in the same manner as described for the STM samples. After incubation, both STM and IR samples were directly analyzed without rinsing.

Surface-enhanced Raman spectroscopy (SERS) was performed on a Renishaw confocal Raman microscope (Renishaw, Inc., Hoffman Estates, Illinois) configured with a laser at 514 nm wavelength, using WiRE 3.2 (Renishaw, Inc.) for spectral processing and analysis. Two substrates designed for surface enhancement were used in this work: Au{111}/mica with nanohole arrays and nanostructured Au on glass. The nanohole arrays (175 nm diameter, 300 nm periodicity) on Au{111}/mica were fabricated using a focused ion beam.[50] The nanostructured Au on glass substrates were made by evaporating 50 Å thick Au at 1 Å/s onto a glass slide and annealing at 400 °C for 24 h. All of the SERS substrates were annealed and incubated in the same manner as the STM/IR samples.

The gold substrates for the XPS, NEXAFS spectroscopy, and RAES experiments were prepared by polished single-crystal Si(100) wafers (Silicon Sense) primed with a 10 nm chromium adhesion layer. The resulting metal films were polycrystalline with grains exhibiting the (111) orientation and sizes of 20−50 nm. After preparation of the cyanide monolayers (see above), the samples were put into glass containers and stored under an inert gas atmosphere until characterization at the synchrotron (see below). The measurements were performed at room temperature and under ultrahigh vacuum conditions (base pressure $<1.5 \times 10^{-9}$ mbar). The spectral acquisition time at a particular sample spot was kept sufficiently short to avoid possible damage by the primary X-rays occurring during the measurements.[51,52]

The experiments were performed at the HE-SGM beamline (bending magnet) of the synchrotron storage ring BESSY II in Berlin, Germany, and at the D1011 beamline (bending magnet, plane grating monochromator) of the MAX II storage ring at the MAX-IV laboratory in Lund, Sweden. The experimental stations at both facilities were equipped with a Scienta electron energy analyzer (R3000 at HE-SGM and SES200 at D1011) and a partial electron yield (PEY) detector. All experimental

DOI: 10.1021/acs.jpcc.6b06006
J. Phys. Chem. C 2016, 120, 26736−26746

adjustments were exactly the same at both beamlines, except for somewhat better energy resolution at D1011 (~70 meV vs ~0.3 eV at HESGM) and a minor difference in the polarization factor of the primary X-ray light, viz., 91% at HESGM and 95% at D1011. The experiments were repeated several times with the same results within experimental error. Independent sets of samples were used.

X-ray photoelectron spectra were recorded with a normal emission geometry at excitation energies of 350 and 580 eV. Synchrotron light was used as the primary X-ray source. The binding energy (E_B) scale of the spectra was referenced to the Au $4f_{7/2}$ peak at E_B = 84.0 eV.[53] The spectra were fit by symmetric Voigt functions and a Shirley-type background.[43]

The acquisition of the NEXAFS spectra was carried for the carbon and nitrogen regions in the PEY mode with retarding voltages of −150 and −300 V, respectively. Linearly polarized synchrotron light was used as the primary X-ray source. The incidence angle of X-rays was varied from 90° (**E** vector in the surface plane) to 20° (**E** vector near the surface normal) in steps of 10−20° to monitor the molecular orientation in the SAMs. This approach is based on the dependence of the cross section of the resonant photoexcitation process on the orientation of the electric field vector of the synchrotron light with respect to the molecular orbital of interest (so-called linear dichroism in X-ray absorption).[54] The energy scale was calibrated by means of the most intense π^* resonance of highly oriented pyrolytic graphite at 285.38 eV[55] in combination with the well-known $\Delta h\nu \propto (h\nu)^{3/2}$ behavior of plane grating monochromators.[56]

The RAES spectra were acquired using either a Scienta R3000 electron energy analyzer (BESSY II) or a SCIENTA SES200 spectrometer (Max-lab). The X-ray incidence angle was set to 55° to suppress possible orientational effects;[54] the takeoff geometry of the electrons was close to normal emission. Resonant excitation was performed at the nitrogen K-edge, at the position of the π(CN*) resonance. The excitation energy was determined in the preliminary NEXAFS experiments. In addition, nonresonant Auger electron spectra were recorded at an excitation energy of 5−6 eV above the absorption edge. This setting was mimicked from similar experiments on nitrile-substituted SAMs on Au{111}, where it was found to be optimal in order to maximize the signal-to-noise ratio and to avoid appearance of interfering gold photoemission in the spectra.[25] Finally, for every sample, a reference spectrum for the pre-edge excitation was measured. This spectrum was subtracted from the RAES and nonresonant AES spectra to correct them for a contribution to the photoemission that could not be avoided completely.

RESULTS

Scanning Tunneling Microscopy—Molecular Resolution of Surface Structure. The STM image in Figure 1a shows the structural details of monolayers of cyanide formed from exposure of Au{111} to HCN(g) at room temperature and humidity, most likely due to the established gold cyanidation redox reaction that involves water and oxygen.[33,44] In comparison to the relatively featureless AuCN monolayers on Au{111} in solution, which are formed through electrochemical deposition,[57] cyanide molecules deposited in this manner are arranged into numerous, highly ordered domains, one-atom-deep substrate vacancy islands, and one-atom-high substrate mesas. At this resolution, the surface morphology closely resembles alkanethiol SAMs, which are also observed to

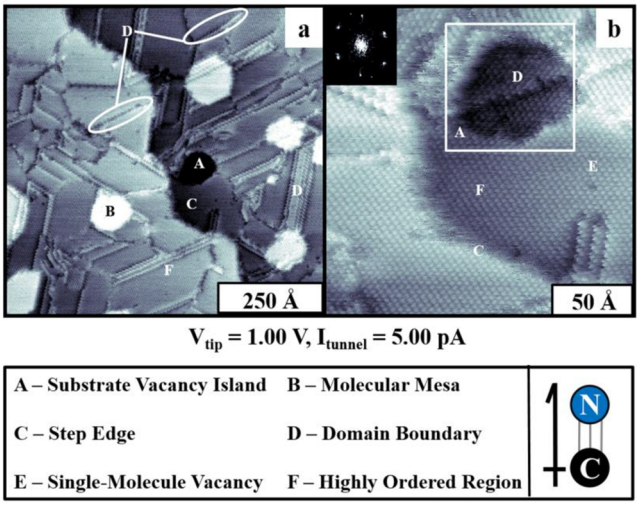

Figure 1. Scanning tunneling microscope images of the surface structure of cyanide monolayers on Au{111} at room temperature. (a) The morphology of the cyanide monolayers with representative surface structures denoted by letters A−F in the image and schematic of cyanide with aligned dipole C → N, positive → negative. (b) Molecular resolution images and corresponding Fourier transform showing the hexagonally close-packed lattice with a nearest neighbor distance of 3.8 ± 0.5 Å.

form hexagonally close-packed (hcp) lattices that contain single-substrate-atom-deep vacancy islands and domain boundaries[4,11,45] with the exception of the mesas and the simpler domain boundary structures here. The observed loss of the Au{111} herringbone structure and the appearance of vacancy islands indicate removal of the reconstruction of the underlying gold lattice and the relatively strong molecule−substrate interactions.[4,11,45,58] This change is not surprising; the thiolate Au−S bond reported at ~2 eV[4,45] is weaker than the Au−C bond reported at >2.4 eV,[59,60] and the alkanethiol system also removes the reconstruction of the underlying Au{111} lattice.[4,11,45] Note that the existence of a strong dipole of the cyanide molecule[61] (positive → negative, C → N, see schematic in Figure 1) axis is a significant property difference from alkanethiol monolayers on Au{111} that can be leveraged to elucidate dipole-mediated interactions.[23,62,63]

Higher resolution images (Figure 1b) reveal the arrangement of individual molecules that are positioned in a hcp arrangement. In addition to the previously mentioned structures, missing single-molecule vacancies can be observed in the molecular lattice. A Fourier transform of the STM image in Figure 1b (inset) shows a hexagonal lattice with the first-order reciprocal lattice spots displayed. The distance from the center in Fourier space to one of the frequency modes corresponds to an average measured nearest neighbor distance of 3.8 ± 0.5 Å and was obtained using measurements from >50 images of different sample regions from >10 different samples. These measurements agree well with reported Au−Au bond spacing in gold−cyanide crystals.[36,38,64] All images were obtained and calibrated against a known SAM of decanethiol on Au{111} before and directly after imaging cyanide to minimize measurement error. Using the calculated nearest neighbor spacing, the Au lattice spacing of 2.89 Å, and the hcp arrangement, the surface packing density for cyanide on Au{111} was calculated to be approximately 1 CN molecule per 1.3 Au atoms. This result differs slightly from the bonding

DOI: 10.1021/acs.jpcc.6b06006
J. Phys. Chem. C 2016, 120, 26736−26746

configuration in most coordination complexes composed of gold and cyanide where multiple cyanide molecules bind to one gold atom.

The specific rotational orientation of the monolayer with respect to the underlying gold lattice is determined with respect to the close-packed direction of the Au{111} formed along straight step edges.[65] The schematic in Figure 2 uses dark

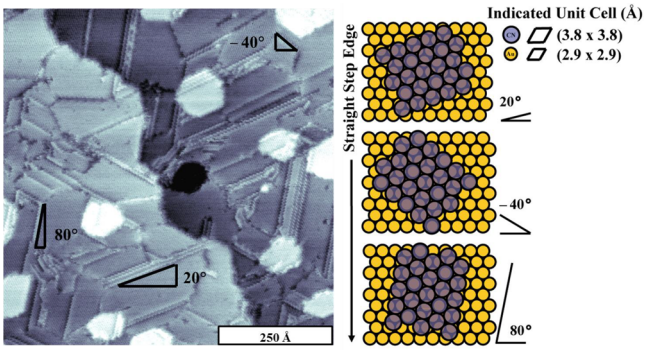

Figure 2. Scanning tunneling microscope image of CN on Au{111} as deposited at room temperature and structural schematics. Using the Au close-packed substrate direction with respect to straight step edges (⟨0 1 0⟩), we find molecules bind to bridge and atop positions with a (3.8 Å × 3.8 Å) cyanide unit cell at 20, −40, and 80° orientations with respect to the unreconstructed underlying gold lattice. The dark, larger circles represent the projection of the cyanide molecules on the smaller circles representing the atoms of the Au{111} lattice. Triangles representing examples of the identified orientations relative to the Au{111} lattice are aligned with cyanide domain boundaries and are identified as high-symmetry directions representative of the hexagonally close-packed arrangement.

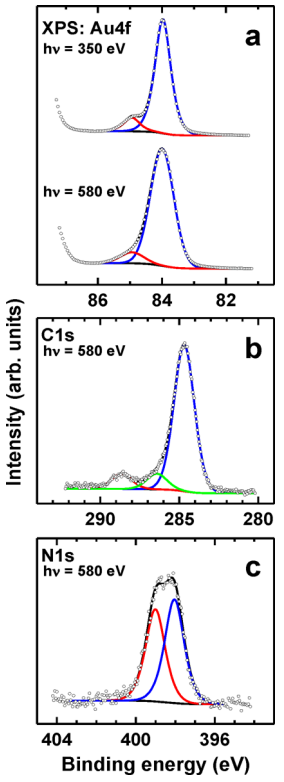

Figure 3. Au $4f_{7/2}$ (a), C 1s (b), and N 1s (c) X-ray photoelectron spectra of NC/Au{111} acquired at photon energies of either 350 or 580 eV as marked in the panels (open circles). The spectra are fit and decomposed into individual contributions (thin solid lines). See text for details.

circles to represent the space-filling projection of the cyanide molecules on the surface using the spatial measurements from the STM images. We find at the 20, −40, and 80° in-plane rotations with respect to the underlying gold lattice that bound cyanide molecules primarily occupied the twofold bridge site with the remaining minority aligned with atop positions. The twofold bridge location has been calculated to be one of the most stable surface locations based on DFT calculations for cyanide bonding to Au{100}, Au{110}, and Au{111}.[66] These in-plane orientational rotations are identified as black triangles in the STM image included in Figure 2 when aligning with monolayer domain boundaries and can be seen to be examples of high symmetry points maintaining the characteristic 60° rotations of the hcp arrangement. In comparison, all other angles introduced binding at threefold hollow sites, reduced the number of twofold bridges, and were observed less frequently than these other rotations in STM images via domain boundary inspection.

X-ray Photoelectron Spectroscopy—Surface Elemental Analysis. Representative Au $4f_{7/2}$, C 1s, and N 1s XPS spectra of NC/Au{111} are shown in Figure 3. The Au $4f_{7/2}$ spectra in Figure 3a exhibit a weak shoulder at the high E_B side of the main emission, at E_B = 84.95 eV. The appearance of this shoulder is attributed to the effect of adsorbed NC, which is strong and, in its extent, is similar to the oxidation of the gold substrate.[67] Significantly, only the topmost layer of the Au{111} substrate is affected, as seen from the direct comparison of the spectra acquired at PEs of 350 and 580 eV in Figure 3a. Due to the strong dependence of the sampling depth of XPS on the kinetic energy of photoelectrons,[68] the contribution of the surface as compared to the bulk should be much weaker in the latter case and, indeed, the high E_B shoulder decreases significantly in intensity at a PE of 580 eV as compared to 350 eV. Further, the intensity relation between the shoulder and the main emission in the 350 eV spectrum can be compared to the analogous relation in the spectrum of clean Au{111}, where the contributions of the topmost layer and the bulk can be straightforwardly distinguished.[52] Accordingly, the shoulder is indeed exclusively related to the topmost layer of the Au{111} substrate, corresponding, according to its spectral weight, to 25−30% of atoms in this layer.[69]

The C 1s XP spectrum of NC/Au{111} in Figure 3b exhibits strong emission at ∼284.7 eV accompanied by two weak peaks at ∼286.4 and ∼288.65 eV. The dominant emission can be assigned to the adsorbed NC molecules, while the low intensity peaks presumably stem from contamination, most likely CO (∼286.4 eV) and COOH (∼288.65 eV).[70] Such contamination can hardly be avoided considering the ultimate thinness of the NC monolayer and its exposure to ambient in the course of the sample handling. However, the formation of well-ordered monolayers, as indicated by the STM images, suggests that such contamination is inconsequential. As to dominant emission, note for comparison that, as expected, its E_B is much lower than that of the nitrile carbon in SAMs of the nitrile-substituted alkanethiols, NC−$(CH_2)_n$−SH (NC−Cn) on Au{111}, e.g., 286.2 eV at n = 3.[30] The lower E_B in the case of NC/Au{111} can be attributed to the direct bonding of NC to the substrate (chemical shift) as well as to more efficient screening of the photoemission hole by the substrate electrons (the screening

DOI: 10.1021/acs.jpcc.6b06006
J. Phys. Chem. C 2016, 120, 26736−26746

effect scales according to the Coulomb potential, i.e., is proportional to $1/r$).

The N 1s XP spectrum of NC/Au{111} in Figure 3c exhibits a broad peak that can be tentatively decomposed into two individual emissions at ~398.1 and ~399.0 eV, with the former emission being more intense. This emission can be unequivocally attributed to the CN molecules attached to the substrate over the C−Au bond. The E_B of 398.1 eV correlates well with the respective E_B for the NC-alkyl SAMs on Au{111}, viz., 398.84 eV for the NC−C_2H_4S film and 398.98 eV for the NC−C_3H_6S monolayer,[30] being noticeably smaller than these values because of the stronger proximity on CN to the substrate in the case of NC/Au{111} (see discussion regarding the C 1s spectrum). The value of ~399.0 eV is even higher than the value of 398.84 eV for the NC−C_2H_4S film on Au{111}, suggesting that the respective species are bound only weakly to the substrate, probably in a physisorbed fashion, or, most likely, CNH or CN−H_2O species. It is well-known that the protonation or association with H_2O shifts the N 1s binding energy to higher values.[71−73] The C atom attached directly to the metal substrate will not be affected strongly by this process, resulting in only a small binding energy shift and, consequently, in only one joint C 1s emission.

Vibrational Spectroscopy—Connectivity. To determine the chemical state and identity of cyanide molecules on Au{111}, we utilized attenuated total internal reflection Fourier transform infrared spectroscopy (ATR-FTIR). The IR absorption spectrum of Au{111} after exposure to HCN(g) is shown in Figure 4. The primary CN stretching mode, as shown in the inset of Figure 4, detected at 2146 cm^{-1} on the Au{111} is in good agreement with spectra for cyanide adsorbed on the surface of gold electrodes in a cyanide solution.[73] It is red-shifted when compared to the 2200−2300 cm^{-1} range given for the nitrile functional group,[74] and shows the typical blue shift due to substrate coupling from the approximately 2080 cm^{-1} for the free cyanide ion in solution[73,75,76] (see Table 1 for comparisons). We observed two small side peaks at 2134 and 2161 cm^{-1} on the Au{111} surface using ATR-FTIR, which is more sensitive to thin films, on either side of the larger, distinct CN stretch at 2146 cm^{-1}.

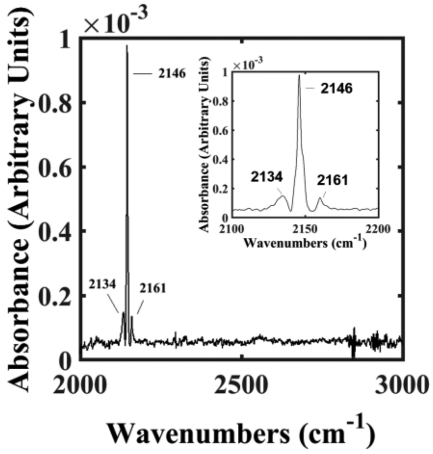

Figure 4. Attenuated total reflection Fourier transform infrared spectrum of CN/Au{111} using custom sapphire prism substrates and showing the CN stretch at 2146 cm^{-1} along with two side peaks at 2134 and 2161 cm^{-1}. The inset is an enlargement of the region of the spectrum containing the CN vibration.

These two additional modes are also likely attributed to the CN stretch, supporting the nitrogen XPS results suggesting different surface states exist for cyanide molecules on the surface. The asymmetric side peaks are not detected for CN adsorbed on polycrystalline Au[73] most likely because the same amount of order cannot be achieved due to the amorphous nature of the surface (see Supplementary Figure S1 and Figure S2 for more detailed comparisons).

No vibrational modes were identified near 3300 cm^{-1} for the CH vibrational mode of the HCN molecule (also shown in Table 1).[77] This observation is consistent with deprotonation during monolayer formation. All spectral measurements were recorded with a bare Au surface as a reference that showed no peaks in the region of interest; peak locations were reproducible over different samples and days.

Raman spectroscopy was used to detect low-frequency, substrate−adsorbate binding modes and the high-frequency internal stretching mode. The Raman spectra for Au{111} and polycrystalline Au nanoparticles (NPs) after exposure to HCN(g) are shown in Figure 5a and b, respectively. The low-frequency modes detected around 304 and 400 cm^{-1} (see Figure 5c inset, Table 1 for comparisons) agree well with values reported for a Au−C stretch and a Au−C−N bend for cyanide ions adsorbed on both Au electrode surfaces in cyanide-ion-containing solution[78] and cyanide-coated gold nanoparticles.[76] No modes were detected in the 100−250 cm^{-1} region that is detected in linear chains of AuCN and are attributed to the CN−Au vibrational mode in solid AuCN.[64] However, we were only able to detect the low-frequency modes on the custom Au NP SERS surface, as the signal-to-noise ratio was much better on the Au NPs. The results are further evidence that the cyanide assembles here attached through Au−C bonds, and not through nitrogen, maintaining the typical bonding scheme for gold−cyanide coordination complexes.[33,38]

The high-frequency mode located at 2140 cm^{-1} for the Au NPs detected by Raman spectroscopy compares well with the detected IR mode for the Au{111} substrate but is blue-shifted by 25 cm^{-1} when compared to the peak at 2165 cm^{-1} detected by Raman spectroscopy for CN/Au{111} and red-shifted when compared with the 2248 cm^{-1} reported for the Raman spectra of the nitrile functional group.[79] The comparison with the nitrile group demonstrates that there is a significant difference in the balance between substrate−molecule and molecule−molecule interactions resulting from direct attachment to the Au surface. An additional peak, which is further evidence of different cyanide states, was located in the CN/Au{111} spectrum at 2235 cm^{-1}, a value that closely matches values reported for CN in solid AuCN crystals.[64] We note that all the Raman shifts detected on the polycrystalline Au NPs are blue-shifted ~20 cm^{-1} compared to cyanide molecules adsorbed on Au{111}. The results presented here may be more accurate, as they are not complicated by dissolving the gold into the surrounding solution or applied electric fields.

Near-Edge X-ray Absorption Fine Structure Spectroscopy—Molecular Orientation. C and N K-edge NEXAFS spectra of NC/Au{111} acquired at an X-ray incident angle of 55° are presented in Figure 6, along with the respective difference between the N K-edge spectra collected under the normal (90°) and grazing (20°) incidence geometry. Note that the "magic angle", 55° spectra are free of orientational effects and, subsequently, only representative of the electronic structure of the studied systems.[54] In contrast, the difference between the spectra acquired at normal and grazing incidence

DOI: 10.1021/acs.jpcc.6b06006
J. Phys. Chem. C 2016, 120, 26736−26746

Table 1. Comparison of the Different Vibration Energies for the Cyanide/Nitrile Group as a Ligand at Solution and Air Interfaces

substance	CN triple bond stretch (cm^{-1})	CH single bond stretch (cm^{-1})	CN triple bond Raman shift (cm^{-1})	Au−C−N Raman shift (cm^{-1})	Au−C Raman shift (cm^{-1})	ref
CN/Au, solution	2105	N/A[a]	2135	300	380	73, 78
$Au(CN)_2^-$, solution	2146	N/A	2156	294	371	73, 76
AuCN, solid/crystal	2236	N/A	2230	358	598	64
HCN, gas	2089	3312	N/A	N/A	N/A	77
CN^-, solution	2080	N/A	N/A	N/A	N/A	73, 75, 76
CN/Au, air[b]	2146	none	2140−2165, 2235	304	400	N/A
CN (nitrile)	2200−2300	2900−3000	2248	N/A	N/A	74, 79

[a]N/A - not applicable. [b]Results presented here.

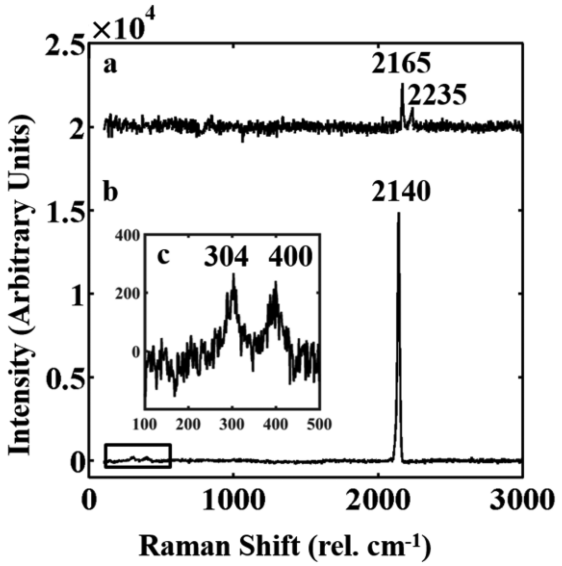

Figure 5. (a) Raman spectra of CN monolayers formed on Au{111} using a plasmonic nanohole array and (b) surface-enhanced Raman substrates made of polycrystalline Au nanoparticles evaporated onto glass. (c) The inset shows both the low frequency modes attributed to the substrate−molecule bond, Au−CN bend at 304 cm^{-1}, and Au−CN stretch at 400 cm^{-1}, which were only detected on the Au nanoparticles.

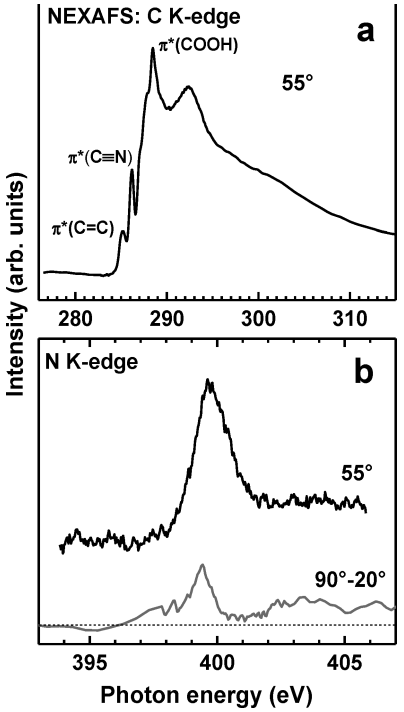

Figure 6. C (a) and N (b) K-edge near-edge X-ray absorption fine structure spectra of NC/Au{111} acquired at an X-ray incident angle of 55° (black solid curves), along with the respective difference between the spectra collected under the normal (90°) and grazing (20°) incidence geometry (gray solid curve in panel b). The characteristic absorption resonances are marked. The horizontal dashed line in panel b corresponds to zero intensity.

of X-rays are representative of the molecular orientation, averaged over the probed ensemble, relying on the linear dichroism effect in X-ray absorption.[54]

The C K-edge spectrum of NC/Au{111} in Figure 6a exhibits several absorption resonances superimposed onto the absorption edge. These features include the π^*(C═C) resonance at 285.1 eV, the π(C*≡N) resonance at 286.2 eV, and the π^*(COOH) at 288.5 eV (the assignments were made according to refs 30 and 53). The π^*(C═C) and π^*(COOH) features stem from contamination, while the π(C*≡N) resonance is characteristic of the CN groups and is attributed to two (almost) degenerate, mutually orthogonal π(C≡N) orbitals.[25,27] Its position depends only weakly on the chemical state of the CN group (unless there is π^*—π^* hybridization with the adjacent functional group)[28] and, in particular, does not vary much across the NC-alkyl/Au{111} series, being 286.8−286.9 eV.

The 55° N K-edge spectrum of NC/Au{111} in Figure 6b exhibits a characteristic π^* resonance of the nitrile group at 399.7 eV. Similar to the π(C*≡N) resonance, it is attributed to two (almost) degenerate, mutually orthogonal π(C≡N) orbitals.[25,27] The presence of this feature as well as the π(C*≡N) resonance at the C K-edge (see above) suggests an upright orientation of the NC moieties in NC/Au{111}. Otherwise, both π(C*≡N) and π(C≡N*) resonances would be quenched through the direct interaction with the substrate and be imperceptible in the spectra. The energy of the π(C≡N*) resonance for NC/Au{111} is close to the analogous value for the NC-alkyl SAMs on Au{111}, viz., 399.75 eV (independent of chain length).[30]

The 90−20° difference spectrum in Figure 6b exhibits a pronounced, positive peak at the position of the π(C≡N*) resonance, suggesting, in view of the orientation of the respective molecular orbitals (perpendicular to the C≡N axis), an upright orientation of the nitrile groups in NC/Au{111}.

Resonant Auger Electron Spectroscopy—Molecule−Substrate Charge-Transfer Efficiency. Nitrile groups have been used before as the starting point for electron transfer (ET)

DOI: 10.1021/acs.jpcc.6b06006
J. Phys. Chem. C 2016, 120, 26736−26746

through the molecular framework in SAMs on conductive substrates.[12,25,27−30] These functional groups were attached to the molecular backbone as a tail moiety at the SAM−ambient interface, while the molecules were coupled to the substrate, Au{111}, by the thiolate anchors. The ET was triggered by the resonant excitation of the N 1s electron into the π(C≡N*) orbital and monitored by RAES within the core−hole clock (CHC) approach.[80−84] Within this approach, different de-excitation channels of the [N 1s]π* state are followed, viz., the emission of the excited electron (participator channel, P), emission of another electron from the occupied valence molecular orbital (spectator channel, SP), and ET of the excited electron to the substrate, all accompanied by an interband transition from the occupied valence molecular orbital to the N 1s hole. The P and SP processes, which are the standard de-excitation routes for RAES, result in one hole (1h) and two-hole one-electron (2h1e) states, respectively (see ref 29 for details and a schematic illustration of the relevant processes). In contrast, the ET scenario results in a 2h state, which is almost identical to the final state of nonresonant Auger electron emission processes.[85] Due to the different final states, all of the above processes have different spectroscopic signatures in the overall RAES spectrum, which can be distinguished and the ET contribution, P_{ET}, precisely extracted. Consequently, the characteristic ET time, τ_{ET}, can be evaluated using the major formula of the CHC approach, viz., $\tau_{ET} = \tau_{core}(1 - P_{ET})/P_{ET}$, where τ_{core} is the core−hole lifetime serving as an internal clock for the ET process and giving the name to the approach.[81] This lifetime is 6.4 fs for the N 1s core hole,[80] providing access to the femtosecond time domain without use of any complex experimental setup relying on pump−probe techniques.

The length of the molecular backbone in the CHC experiments on nitrile-substituted SAMs was varied, with P_{ET} increasing and τ_{ET} decreasing progressively with decreasing backbone length.[28−30] In particular, τ_{ET} varied from 100 ± 26 fs for NC−C_4H_8S/Au to 35 ± 9 fs for NC−C_3H_6S/Au to 14 ± 4 fs for NC−C_2H_4S/Au.[30] Further, in the extrapolated limit of the negligible short backbone, the characteristic time for ET from the NC group directly attached to the thiolate anchor to the substrate was found to be ∼2.3[30] and ∼2.8 fs[28] in the independent experiments on different systems, being ∼2.5 fs on average. In this context, NC/Au{111} represents a further, ultimate case, with the exclusion of the "intermediate" thiolate moiety and direct attachment of the nitrile group to Au{111} with a C−Au bond. Under these circumstances, ET to the substrate should be especially efficient, representing, most likely, the major de-excitation channel of the [N 1s]π* state.

This efficient ET to the substrate is indeed the case, as shown in Figure 7, where the [N 1s]π* resonant Auger electron spectra (RAES) and corresponding Auger electron spectra (AES) for NC/Au{111} are presented, along with the analogous data for NC−C_2H_4S/Au{111},[25,30] for comparison. The RAES spectra of NC−C_2H_4S/Au{111} are dominated by the SP and P contributions, while the ET part, shown separately, contributes only ∼30% of the entire spectral weight. In contrast, the RAES and AES spectra of NC/Au{111} are almost identical, suggesting that the former spectra are dominated by the ET contribution, while the SP and P parts are barely perceptible. Taking the RAES spectrum of NC−$C_{16}H_{32}$S/Au{111} as the reference for the purely resonant (autoionization) spectrum[25,30] and the nonresonant AES spectrum of NC/Au{111} as the representative for the ET

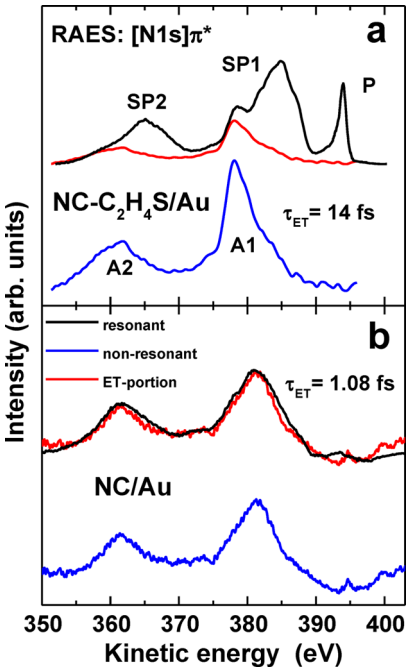

Figure 7. [N 1s]π* resonant Auger electron spectra (RAES, black curves) and nonresonant Auger electron (blue curves) spectra of NC−C_2H_4S/Au (a) and NC/Au{111} (b). The electron transfer contribution in the resonant Auger electron spectra is shown (red curves). P, SP1, and SP2 denote the participator and two spectator features, respectively. A1 and A2 denote two characteristic features in the nonresonant spectra. The derived τ_{ET} are given. The spectra of NC−C_2H_4S/Au are reprinted with permission from ref 30. Copyright 2010 American Chemical Society.

process (see above), the RAES spectrum of NC/Au{111} can be decomposed into the SP/P and ET contributions and τ_{ET} can be calculated according to the major formula of the CHC approach (see above). Three independent sets of experiments resulted in τ_{ET} values of 0.25, 1.08, and 1.38 fs, giving 0.9 fs on average. The accuracy of this value is ±0.5 fs from the statistical viewpoint and ±0.25 fs based on the accuracy of the τ_{core} value.[80] The comparison of this value with the analogous values for NC−$(CH_2)_2$S/Au is given in Figure 8. The most important feature, however, is the dominance of the ET process over the SP/P contributions in the [N 1s]π* decay spectrum of NC/Au{111}, suggesting strong coupling to the substrate. Another important result, is an ultimate proof for the CHC approach in its specific application to SAMs, based on the resonantly addressable NC group.[12,25,27−30] Indeed, as can be expected, the value of τ_{ET} for the direct attachment of the nitrile group to the Au{111} substrate is noticeably smaller than that for any molecular backbone, e.g., 14.4 fs for NC−C_2H_4S/Au[25,30] and 9 ± 3 fs for SAMs of NC−C_6H_4−SH/Au{111},[28] fitting well to the proposed exponential dependence of τ_{ET} on the length of the alkyl chain derived from the NC−$(CH_2)_n$S/Au data (Figure 8a). The τ_{ET} for NC/Au{111} is somewhat smaller than the characteristic time for n = 0, obtained from the intercept of the ln τ_{ET} plot with the y-axis, viz., 2.3 fs[30] (2.8 fs in ref 28). This result is understandable, since the latter value, $\tau_{n=0}$, is associated with both the ET time required for transfer from the NC group to the backbone and the ET time required for transfer from the backbone to the substrate. Assuming that the former contribution is close to τ_{ET} for NC/Au{111}, the latter time can be coarsely estimated at ∼1.3 fs. This value is comparable

DOI: 10.1021/acs.jpcc.6b06006
J. Phys. Chem. C 2016, 120, 26736−26746

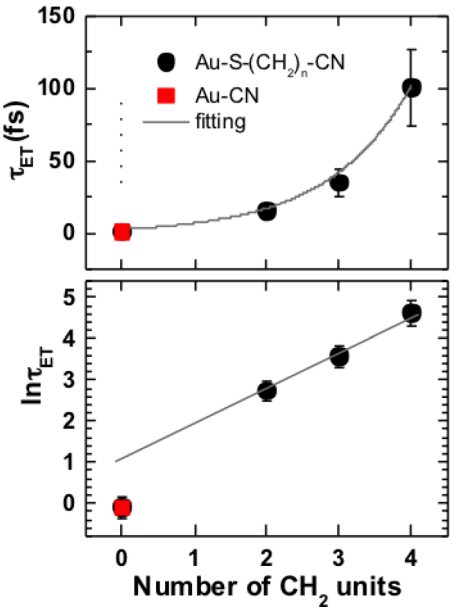

Figure 8. Electron transfer (ET) time (top panel) from the excited NC group to the substrate and its natural logarithm (bottom panel) for NC/Au (red square) and NC−$(CH_2)_n$S/Au (n = 2−4; black filled circles) versus the number (n) of methylene (CH_2) units in the aliphatic chain. The gray solid lines in the top and bottom panels represent the best exponential and linear fits, respectively. The intercept of the ln τ_{ET} plot with the y-axis corresponds to the ET time required for transfer from the NC group to the backbone plus the ET time required for transfer from the backbone to the substrate. The intercept of 0.83 gives a $\tau_{n=0}$ value of 2.3 fs. The values for NC−$(CH_2)_n$S/Au are reprinted with permission from ref 30. Copyright 2010 American Chemical Society.

to a characteristic time of ∼320 as (0.32 fs) observed for ET from an adsorbed sulfur atom to the substrate in the c(4 × 2)-S/Ru(0001) system.[84] The difference, which is reasonably small, can be explained by band alignment differences, the stronger bonding of the S atoms to the substrate in the latter case, as well as the different characters of the involved orbitals serving as the starting point for ET in both cases. It is well-known that the character of the primary molecular or atomic orbital affects the efficiency of ET.[27,28]

Discussion of Results—Bonding Scheme and Substrate−Molecule Coupling. Combining our structural and spectroscopic measurements with known Au−cyanide chemistry, we propose a bonding scheme for cyanide monolayers on Au{111}. Assuming that the molecules on the surface organize to maximize intermolecular interactions for monolayer stability, and to offset unfavorable dipole coupling,[73] we propose a bonding scheme where the cyanide molecules are bound via a Au−C bond and are oriented normal to the surface. Note that when cyanide is attached to a carbon backbone as a nitrile group it has an inclined orientation measured around 65°,[3,30] suggesting that the strength of the substrate−molecule bond is dominant over the intermolecular interactions and overpowers the unfavorable dipole−dipole interactions.

Finally, from the CHC results measuring the ∼1 fs charge transfer from the cyanide directly to the gold, as shown schematically in Figure 9, we can infer that the electronic coupling is particularly strong between the carbon and gold based on the facile electron transfer. This result directly supports the expected dominance of σ bonding suggested by

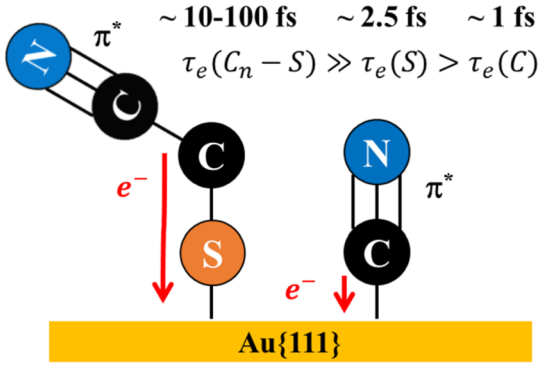

Figure 9. Electron transfer across the Au−C bond is extremely efficient at ∼1 fs, indicating strong electronic coupling between substrate and molecule.

the increase in CN vibrational frequency. The electron transfer efficiency, coupled with the molecule orientation, is an indication that there is a favorable energetic overlap between the molecular transport orbitals and substrate Fermi level[24] and follows the trend for electron transfer time as a function of the length of the carbon backbone in nitrile functionalized alkanethiol SAMs previously shown in Figure 8.[30] In fact, complementary to these results, it has been reported that the conduction efficiency is significantly lower for isocyanide or Au−NC bound molecules.[31]

■ CONCLUSIONS AND PROSPECTS

The vibrational and structural characteristics of stable cyanide monolayers on Au{111} are revealed, and we show that coupling to the gold substrate is particularly strong, leading to facile electron transfer. Cyanide molecules form a hexagonal close-packed lattice with a nearest neighbor spacing of 3.8 ± 0.5 Å. It was discovered using ATR-FTIR and SERS that the cyanide molecules are attached to the gold through the carbon atom and oriented normal to the surface. The molecular composition and orientation was supported by high-resolution XPS (HRXPS) and NEXAFS spectroscopy, and we discuss a bonding scheme that compares favorably with the structure observed in the STM images. The CHC method of RAES measured the charge transfer from the cyanide to the gold to be below 1 fs, comparable to charge transfer across the sulfur bond of thiols and 100 times faster than when an alkane backbone is present. These results further validate the use of the core−hole clock method for measuring the ultrafast process of electron transfer between molecule and substrate for self-assembled monolayers. Current research is aimed at exploiting the strong dipole moment of cyanide, molecule orientation, and the strength of the molecule−substrate electronic coupling for probing the interactions between molecular electronic states and molecular vibrations at room temperature, which is critical to developing more generally applicable single-molecule spectroscopic techniques.

■ ASSOCIATED CONTENT

Supporting Information

The Supporting Information is available free of charge on the ACS Publications website at DOI: 10.1021/acs.jpcc.6b06006.

Data and figures of details of infrared spectra of CN on Au{111} (PDF)

DOI: 10.1021/acs.jpcc.6b06006
J. Phys. Chem. C 2016, 120, 26736−26746

AUTHOR INFORMATION

Corresponding Authors

*E-mail: dla3@psu.edu.
*E-mail: michael.zharnikov@urz.uni-heidelberg.de. Phone: +49-6221-54 4921.
*E-mail: psw@cnsi.ucla.edu. Phone: +1 (310) 825-0317.

Notes

The authors declare no competing financial interest.

ACKNOWLEDGMENTS

The authors thank the Department of Energy Grant No. DE-SC-1037004 for support of this work. M.Z. and T.W. appreciate financial support of the German Research Foundation (DFG), grant ZH 63/14-2. We thank Dr. Huan Cao, Dr. Nathan Hohman, Prof. Wei-Ssu Liao, Dr. Jeffrey Schwartz, Andrew Serino, Dr. Liane Slaughter, and Dr. John Thomas for helpful scientific discussions. T.W. and M.Z. thank Helmholtz Zentrum Berlin (HZB) and Max-IV Laboratory for the allocation of synchrotron radiation beam time and Dr. A. Nefedov and Prof. Dr. Ch. Wöll (KIT) for technical cooperation at BESSY II (HZB).

REFERENCES

(1) Netzer, L.; Iscovici, R.; Sagiv, J. Adsorbed Monolayers versus Langmuir-Blodgett Monolayers—Why and How? II: Characterization of Built-Up Films Constructed by Stepwise Adsorption of Individual Monolayers. *Thin Solid Films* **1983**, *100*, 67−76.

(2) Stranick, S. J.; Kamna, M. M.; Krom, K. R.; Parikh, A. N.; Allara, D. L.; Weiss, P. S. Scanning Tunneling Microscopy Studies of Self-Assembled Monolayers of Alkanethiols on Gold. *J. Vac. Sci. Technol., B: Microelectron. Process. Phenom.* **1994**, *12*, 2004−2007.

(3) Frey, S.; Shaporenko, A.; Zharnikov, M.; Harder, P.; Allara, D. L. Self-Assembled Monolayers of Nitrile-Functionalized Alkanethiols on Gold and Silver Substrates. *J. Phys. Chem. B* **2003**, *107*, 7716−7725.

(4) Love, J. C.; Estroff, L. A.; Kriebel, J. K.; Nuzzo, R. G.; Whitesides, G. M. Self-Assembled Monolayers of Thiolates on Metals as a Form of Nanotechnology. *Chem. Rev.* **2005**, *105*, 1103−1170.

(5) Weiss, P. S. Functional Molecules and Assemblies in Controlled Environments: Formation and Measurements. *Acc. Chem. Res.* **2008**, *41*, 1772−1781.

(6) Liao, W.-S.; Cheunkar, S.; Cao, H. H.; Bednar, H. R.; Weiss, P. S.; Andrews, A. M. Subtractive Patterning via Chemical Lift-Off Lithography. *Science* **2012**, *337*, 1517−1521.

(7) Kim, J.; Rim, Y. S.; Liu, Y.; Serino, A. C.; Thomas, J. C.; Chen, H.; Yang, Y.; Weiss, P. S. Interface Control in Organic Electronics Using Mixed Monolayers of Carboranethiol Isomers. *Nano Lett.* **2014**, *14*, 2946−2951.

(8) Abendroth, J. M.; Bushuyev, O. S.; Weiss, P. S.; Barrett, C. J. Controlling Motion at the Nanoscale: Rise of the Molecular Machines. *ACS Nano* **2015**, *9*, 7746−7768.

(9) Sykes, E. C. H.; Han, P.; Kandel, S. A.; Kelly, K. F.; McCarty, G. S.; Weiss, P. S. Substrate-Mediated Interactions and Intermolecular Forces between Molecules Adsorbed on Surfaces. *Acc. Chem. Res.* **2003**, *36*, 945−953.

(10) Monnell, J. D.; Stapleton, J. J.; Dirk, S. M.; Reinerth, W. A.; Tour, J. M.; Allara, D. L.; Weiss, P. S. Relative Conductances of Alkaneselenolate and Alkanethiolate Monolayers on Au{111}. *J. Phys. Chem. B* **2005**, *109*, 20343−20349.

(11) Hakkinen, H. The Gold-Sulfur Interface at the Nanoscale. *Nat. Chem.* **2012**, *4*, 443−455.

(12) Ossowski, J.; Wächter, T.; Silies, L.; Kind, M.; Noworolska, A.; Blobner, F.; Gnatek, D.; Rysz, J.; Bolte, M.; Feulner, P.; et al. Thiolate versus Selenolate: Structure, Stability, and Charge Transfer Properties. *ACS Nano* **2015**, *9*, 4508−4526.

(13) Cygan, M. T.; Dunbar, T. D.; Arnold, J. J.; Bumm, L. A.; Shedlock, N. F.; Burgin, T. P.; Jones, L.; Allara, D. L.; Tour, J. M.; Weiss, P. S. Insertion, Conductivity, and Structures of Conjugated Organic Oligomers in Self-Assembled Alkanethiol Monolayers on Au{111}. *J. Am. Chem. Soc.* **1998**, *120*, 2721−2732.

(14) Weck, M.; Jackiw, J. J.; Rossi, R. R.; Weiss, P. S.; Grubbs, R. H. Ring-Opening Metathesis Polymerization from Surfaces. *J. Am. Chem. Soc.* **1999**, *121*, 4088−4089.

(15) Saavedra, H. M.; Thompson, C. M.; Hohman, J. N.; Crespi, V. H.; Weiss, P. S. Reversible Lability by in Situ Reaction of Self-Assembled Monolayers. *J. Am. Chem. Soc.* **2009**, *131*, 2252−2259.

(16) Saavedra, H. M.; Mullen, T. J.; Zhang, P.; Dewey, D. C.; Claridge, S. A.; Weiss, P. S. Hybrid Strategies in Nanolithography. *Rep. Prog. Phys.* **2010**, *73*, 036501.

(17) Kim, M.; Hohman, J. N.; Cao, Y.; Houk, K. N.; Ma, H.; Jen, A. K.-Y.; Weiss, P. S. Creating Favorable Geometries for Directing Organic Photoreactions in Alkanethiolate Monolayers. *Science* **2011**, *331*, 1312−1315.

(18) Cao, H. H.; Nakatsuka, N.; Serino, A. C.; Liao, W.-S.; Cheunkar, S.; Yang, H.; Weiss, P. S.; Andrews, A. M. Controlled DNA Patterning by Chemical Lift-Off Lithography: Matrix Matters. *ACS Nano* **2015**, *9*, 11439−11454.

(19) Kumar, A. S.; Ye, T.; Takami, T.; Yu, B.-C.; Flatt, A. K.; Tour, J. M.; Weiss, P. S. Reversible Photo-Switching of Single Azobenzene Molecules in Controlled Nanoscale Environments. *Nano Lett.* **2008**, *8*, 1644−1648.

(20) Gao, P.; Weaver, M. J. Metal-Adsorbate Vibrational Frequencies as a Probe of Surface Bonding: Halides and Pseudohalides at Gold Electrodes. *J. Phys. Chem.* **1986**, *90*, 4057−4063.

(21) Galperin, M.; Ratner, M. A.; Nitzan, A. Molecular Transport Junctions: Vibrational Effects. *J. Phys.: Condens. Matter* **2007**, *19*, 103201.

(22) Donhauser, Z. J.; Mantooth, B. A.; Kelly, K. F.; Bumm, L. A.; Monnell, J. D.; Stapleton, J. J.; Price, D. W.; Rawlett, A. M.; Allara, D. L.; Tour, J. M.; et al. Conductance Switching in Single Molecules through Conformational Changes. *Science* **2001**, *292*, 2303−2307.

(23) Lewis, P. A.; Inman, C. E.; Maya, F.; Tour, J. M.; Hutchison, J. E.; Weiss, P. S. Molecular Engineering of the Polarity and Interactions of Molecular Electronic Switches. *J. Am. Chem. Soc.* **2005**, *127*, 17421−17426.

(24) Zangmeister, C. D.; Robey, S. W.; van Zee, R. D.; Kushmerick, J. G.; Naciri, J.; Yao, Y.; Tour, J. M.; Varughese, B.; Xu, B.; Reutt-Robey, J. E. Fermi Level Alignment in Self-Assembled Molecular Layers: The Effect of Coupling Chemistry. *J. Phys. Chem. B* **2006**, *110*, 17138−17144.

(25) Neppl, S.; Bauer, U.; Menzel, D.; Feulner, P.; Shaporenko, A.; Zharnikov, M.; Kao, P.; Allara, D. L. Charge Transfer Dynamics in Self-Assembled Monomolecular Films. *Chem. Phys. Lett.* **2007**, *447*, 227−231.

(26) Moore, A. M.; Weiss, P. S. Functional and Spectroscopic Measurements with Scanning Tunneling Microscopy. *Annu. Rev. Anal. Chem.* **2008**, *1*, 857−882.

(27) Blobner, F.; Coto, P. B.; Allegretti, F.; Bockstedte, M.; Rubio-Pons, O.; Wang, H.; Allara, D. L.; Zharnikov, M.; Thoss, M.; Feulner, P. Orbital-Symmetry-Dependent Electron Transfer through Molecules Assembled on Metal Substrates. *J. Phys. Chem. Lett.* **2012**, *3*, 436−440.

(28) Hamoudi, H.; Neppl, S.; Kao, P.; Schüpbach, B.; Feulner, P.; Terfort, A.; Allara, D.; Zharnikov, M. Orbital-Dependent Charge Transfer Dynamics in Conjugated Self-Assembled Monolayers. *Phys. Rev. Lett.* **2011**, *107*, 027801.

(29) Zharnikov, M. Probing Charge Transfer Dynamics in Self-Assembled Monolayers by Core Hole Clock Approach. *J. Electron Spectrosc. Relat. Phenom.* **2015**, *200*, 160−173.

(30) Kao, P.; Neppl, S.; Feulner, P.; Allara, D. L.; Zharnikov, M. Charge Transfer Time in Alkanethiolate Self-Assembled Monolayers via Resonant Auger Electron Spectroscopy. *J. Phys. Chem. C* **2010**, *114*, 13766−13773.

(31) Kiguchi, M.; Miura, S.; Hara, K.; Sawamura, M.; Murakoshi, K. Conductance of a Single Molecule Anchored by an Isocyanide Substituent to Gold Electrodes. *Appl. Phys. Lett.* **2006**, *89*, 213104.

DOI: 10.1021/acs.jpcc.6b06006
J. Phys. Chem. C 2016, 120, 26736−26746

(32) Lauhon, L. J.; Ho, W. Single-Molecule Vibrational Spectroscopy and Microscopy: CO on Cu(001) and Cu(110). *Phys. Rev. B: Condens. Matter Mater. Phys.* **1999**, *60*, R8525−R8528.
(33) Ahmad, S. The Chemistry of Cyano Complexes of Gold(I) with Emphasis on the Ligand Scrambling Reactions. *Coord. Chem. Rev.* **2004**, *248*, 231−243.
(34) McCarley, R. L.; Bard, A. J. Surface Reactions of Gold(111) with Aqueous Cyanide Studied by Scanning Tunneling Microscopy. *J. Phys. Chem.* **1992**, *96*, 7410−7416.
(35) Sun, L.; Crooks, R. M. Indirect Visualization of Defect Structures Contained within Self-Assembled Organomercaptan Monolayers: Combined Use of Electrochemistry and Scanning Tunneling Microscopy. *Langmuir* **1993**, *9*, 1951−1954.
(36) Katz, M. J.; Sakai, K.; Leznoff, D. B. The Use of Aurophilic and Other Metal-Metal Interactions as Crystal Engineering Design Elements to Increase Structural Dimensionality. *Chem. Soc. Rev.* **2008**, *37*, 1884−1895.
(37) Hu, M.; Belik, A. A.; Imura, M.; Yamauchi, Y. Tailored Design of Multiple Nanoarchitectures in Metal-Cyanide Hybrid Coordination Polymers. *J. Am. Chem. Soc.* **2013**, *135*, 384−391.
(38) Kim, K. H.; Kim, J. G.; Nozawa, S.; Sato, T.; Oang, K. Y.; Kim, T. W.; Ki, H.; Jo, J.; Park, S.; Song, C.; et al. Direct Observation of Bond Formation in Solution with Femtosecond X-Ray Scattering. *Nature* **2015**, *518*, 385−389.
(39) Chattopadhyay, S.; Ganguly, A.; Chen, K.-H.; Chen, L.-C. One-Dimensional Group III-Nitrides: Growth, Properties, and Applications in Nanosensing and Nano-Optoelectronics. *Crit. Rev. Solid State Mater. Sci.* **2009**, *34*, 224−279.
(40) Han, P.; Sykes, E. C. H.; Pearl, T. P.; Weiss, P. S. A Comparative Scanning Tunneling Microscopy Study of Physisorbed Linear Quadrupolar Molecules: C_2N_2 and CS_2 on Au{111} at 4 K. *J. Phys. Chem. A* **2003**, *107*, 8124−8129.
(41) Guttentag, A. I.; Barr, K. K.; Song, T.-B.; Bui, K. V.; Fauman, J. N.; Torres, L. F.; Kes, D. D.; Ciomaga, A.; Gilles, J.; Sullivan, N. F.; Yang, Y.; Allara, D. L.; Zharnikov, M.; Weiss, P. S. *J. Am. Chem. Soc.* **2016**, DOI: 10.1021/jacs.6b06046.
(42) Swanson, S. A.; McClain, R.; Lovejoy, K. S.; Alamdari, N. B.; Hamilton, J. S.; Scott, J. C. Self-Assembled Diisocyanide Monolayer Films on Gold and Palladium. *Langmuir* **2005**, *21*, 5034−5039.
(43) Crudden, C. M.; Horton, J. H.; Ebralidze, I. I.; Zenkina, O. V.; McLean, A. B.; Drevniok, B.; She, Z.; Kraatz, H.-B.; Mosey, N. J.; Seki, T.; et al. Ultra Stable Self-Assembled Monolayers of N-Heterocyclic Carbenes on Gold. *Nat. Chem.* **2014**, *6*, 409−414.
(44) Senanayake, G. Kinetics and Reaction Mechanism of Gold Cyanidation: Surface Reaction Model via Au(I)−OH−CN Complexes. *Hydrometallurgy* **2005**, *80*, 1−12.
(45) Ulman, A. Formation and Structure of Self-Assembled Monolayers. *Chem. Rev.* **1996**, *96*, 1533−1554.
(46) Porath, D.; Millo, O.; Gersten, J. I. Scanning Tunneling Microscopy Studies and Computer Simulations of Annealing of Gold Films. *J. Vac. Sci. Technol., B: Microelectron. Process. Phenom.* **1996**, *14*, 30−37.
(47) Bumm, L. A.; Arnold, J. J.; Charles, L. F.; Dunbar, T. D.; Allara, D. L.; Weiss, P. S. Directed Self-Assembly to Create Molecular Terraces with Molecularly Sharp Boundaries in Organic Monolayers. *J. Am. Chem. Soc.* **1999**, *121*, 8017−8021.
(48) Mantooth, B. A. *Nanoscopic Analyses: Single Molecule Characterization in Molecular Electronics and Surface Science*; The Pennsylvania State University: University Park, PA, 2004.
(49) Wakamatsu, T.; Aizawa, K. Penetration-Depth Characteristics of Evanescent Fields at Metal Attenuated Total Reflection. *Jpn. J. Appl. Phys.* **2005**, *44*, 4272.
(50) Zheng, Y. B.; Payton, J. L.; Chung, C.-H.; Liu, R.; Cheunkar, S.; Pathem, B. K.; Yang, Y.; Jensen, L.; Weiss, P. S. Surface-Enhanced Raman Spectroscopy to Probe Reversibly Photoswitchable Azobenzene in Controlled Nanoscale Environments. *Nano Lett.* **2011**, *11*, 3447−3452.
(51) Heister, K.; Zharnikov, M.; Grunze, M.; Johansson, L. S. O.; Ulman, A. Characterization of X-ray Induced Damage in Alkanethiolate Monolayers by High-Resolution Photoelectron Spectroscopy. *Langmuir* **2001**, *17*, 8−11.
(52) Zharnikov, M. High-Resolution X-Ray Photoelectron Spectroscopy in Studies of Self-Assembled Organic Monolayers. *J. Electron Spectrosc. Relat. Phenom.* **2010**, *178−179*, 380−393.
(53) Moulder, J. F.; Chastain, J. *Handbook of X-Ray Photoelectron Spectroscopy: A Reference Book of Standard Spectra for Identification and Interpretation of XPS Data*; Physical Electronics Division, Perkin-Elmer Corporation: Eden Prarie, Minnesota, 1992.
(54) Stöhr, J. *NEXAFS Spectroscopy*; Springer-Verlag: Berlin, Heidelberg, 1992.
(55) Batson, P. E. Carbon-1s Near-Edge-Absorption Fine Structure in Graphite. *Phys. Rev. B: Condens. Matter Mater. Phys.* **1993**, *48*, 2608−2610.
(56) Domke, M.; Mandel, T.; Puschmann, A.; Xue, C.; Shirley, D. A.; Kaindl, G.; Petersen, H.; Kuske, P. Performance of the High-Resolution SX700/II Monochromator. *Rev. Sci. Instrum.* **1992**, *63*, 80−89.
(57) Yamada, T.; Sekine, R.; Sawaguchi, T. Ultrahigh-Vacuum Multitechnique Study of AuCN Monolayers on Au(111) Formed by Electrochemical Deposition. *J. Chem. Phys.* **2000**, *113*, 1217−1227.
(58) Han, P.; Weiss, P. S. Electronic Substrate-Mediated Interactions. *Surf. Sci. Rep.* **2012**, *67*, 19−81.
(59) Wang, X.-B.; Wang, Y.-L.; Yang, J.; Xing, X.-P.; Li, J.; Wang, L.-S. Evidence of Significant Covalent Bonding in $Au(CN)_2^-$. *J. Am. Chem. Soc.* **2009**, *131*, 16368−16370.
(60) Liu, H.-T.; Xiong, X.-G.; Diem Dau, P.; Wang, Y.-L.; Huang, D.-L.; Li, J.; Wang, L.-S. Probing the Nature of Gold−Carbon Bonding in Gold−Alkynyl Complexes. *Nat. Commun.* **2013**, *4*, 2201.
(61) Smyth, C. P.; McAlpine, K. B. The Dipole Moments of Phosgene, Hydrogen Cyanide and Certain Substituted Methanes. *J. Am. Chem. Soc.* **1934**, *56*, 1697−1700.
(62) Thomas, J. C.; Schwartz, J. J.; Hohman, J. N.; Claridge, S. A.; Auluck, H. S.; Serino, A. C.; Spokoyny, A. M.; Tran, G.; Kelly, K. F.; Mirkin, C. A.; et al. Defect-Tolerant Aligned Dipoles within Two-Dimensional Plastic Lattices. *ACS Nano* **2015**, *9*, 4734−4742.
(63) Schwartz, J. J.; Mendoza, A. M.; Wattanatorn, N.; Zhao, Y.; Nguyen, V. T.; Spokoyny, A. M.; Mirkin, C. A.; Baše, T.; Weiss, P. S. Surface Dipole Control of Liquid Crystal Alignment. *J. Am. Chem. Soc.* **2016**, *138*, 5957−5967.
(64) Bowmaker, G. A.; Kennedy, B. J.; Reid, J. C. Crystal Structures of AuCN and AgCN and Vibrational Spectroscopic Studies of AuCN, AgCN, and CuCN. *Inorg. Chem.* **1998**, *37*, 3968−3974.
(65) Dameron, A. A.; Charles, L. F.; Weiss, P. S. Structures and Displacement of 1-Adamantanethiol Self-Assembled Monolayers on Au{111}. *J. Am. Chem. Soc.* **2005**, *127*, 8697−8704.
(66) Beltramo, G. L.; Shubina, T. E.; Mitchell, S. J.; Koper, M. T. M. Cyanide Adsorption on Gold Electrodes: A Combined Surface Enhanced Raman Spectroscopy and Density Functional Theory Study. *J. Electroanal. Chem.* **2004**, *563*, 111−120.
(67) Yan, C.; Gölzhäuser, A.; Grunze, M.; Wöll, C. Formation of Alkanethiolate Self-Assembled Monolayers on Oxidized Gold Surfaces. *Langmuir* **1999**, *15*, 2414−2419.
(68) Ratner, B. D.; Castner, D. G. Electron Spectroscopy for Chemical Analysis. *Surface Analysis − The Principal Techniques*; John Wiley & Sons, Ltd: West Sussex, United Kingdom, 2009; pp 47−112.
(69) Pireaux, J. J.; Liehr, M.; Thiry, P. A.; Delrue, J. P.; Caudano, R. Electron Spectroscopic Characterization of Oxygen Adsorption on Gold Surfaces II. Production of Gold Oxide in Oxygen DC Reactive Sputtering. *Surf. Sci.* **1984**, *141* (141), 221−232.
(70) Cebula, I.; Lu, H.; Zharnikov, M.; Buck, M. Monolayers of Trimesic and Isophthalic Acid on Cu and Ag: The Influence of Coordination Strength on Adsorption Geometry. *Chem. Sci.* **2013**, *4*, 4455−4464.
(71) Zhou, W. P.; Baunach, T.; Ivanova, V.; Kolb, D. M. Structure and Electrochemistry of 4,4′-Dithiodipyridine Self-Assembled Monolayers in Comparison with 4-Mercaptopyridine Self-Assembled Monolayers on Au(111). *Langmuir* **2004**, *20*, 4590−4595.

DOI: 10.1021/acs.jpcc.6b06006
J. Phys. Chem. C 2016, 120, 26736−26746

(72) Zubavichus, Y.; Zharnikov, M.; Yang, Y.; Fuchs, O.; Umbach, E.; Heske, C.; Ulman, A.; Grunze, M. X-ray Photoelectron Spectroscopy and Near-Edge X-ray Absorption Fine Structure Study of Water Adsorption on Pyridine-Terminated Thiolate Self-Assembled Monolayers. *Langmuir* **2004**, *20*, 11022−11029.
(73) Kunimatsu, K.; Seki, H.; Golden, W. G.; Gordon, J. G.; Philpott, M. R. A Study of the Gold/Cyanide Solution Interface by In Situ Polarization-Modulated Fourier Transform Infrared Reflection Absorption Spectroscopy. *Langmuir* **1988**, *4*, 337−341.
(74) Bernstein, M. P.; Sandford, S. A.; Allamandola, L. J. The Infrared Spectra of Nitriles and Related Compounds Frozen in Ar and H_2O. *Astrophys. J.* **1997**, *476*, 932−942.
(75) Jobe, D. J.; Westaway, K. C. Fourier Transform Infrared Spectroscopy Studies of Cyanide Ion Solutions of Dimethylformamide and Aqueous Dimethylformamide. *Can. J. Chem.* **1993**, *71*, 1353−1361.
(76) Senapati, D.; Dasary, S. S. R.; Singh, A. K.; Senapati, T.; Yu, H.; Ray, P. C. A Label-Free Gold-Nanoparticle-Based SERS Assay for Direct Cyanide Detection at the Parts-per-Trillion Level. *Chem. - Eur. J.* **2011**, *17*, 8445−8451.
(77) Keedy, C. R. The Rotational-Vibrational Spectra of HCN and DCN: A Physical Chemistry Experiment. *J. Chem. Educ.* **1992**, *69*, A296.
(78) Pettinger, B.; Picardi, G.; Schuster, R.; Ertl, G. Surface-Enhanced and STM Tip-Enhanced Raman Spectroscopy of CN^- Ions at Gold Surfaces. *J. Electroanal. Chem.* **2003**, *554*−*555*, 293−299.
(79) Neelakantan, P. Raman Spectrum of Acetonitrile. *Proc. - Indian Acad. Sci., Sect. A* **1964**, *60*, 422−424.
(80) Kempgens, B.; Kivimäki, A.; Neeb, M.; Köppe, H. M.; Bradshaw, A. M.; Feldhaus, J. A High-Resolution N 1s Photoionization Study of the N_2 Molecule in the Near-Threshold Region. *J. Phys. B: At., Mol. Opt. Phys.* **1996**, *29*, 5389−5402.
(81) Brühwiler, P. A.; Karis, O.; Mårtensson, N. Charge-Transfer Dynamics Studied Using Resonant Core Spectroscopies. *Rev. Mod. Phys.* **2002**, *74*, 703−740.
(82) Schnadt, J.; Bruhwiler, P. A.; Patthey, L.; O'Shea, J. N.; Sodergren, S.; Odelius, M.; Ahuja, R.; Karis, O.; Bassler, M.; Persson, P.; et al. Experimental Evidence for Sub-3-fs Charge Transfer from an Aromatic Adsorbate to a Semiconductor. *Nature* **2002**, *418*, 620−623.
(83) de Jong, M. P.; Friedlein, R.; Sorensen, S. L.; Öhrwall, G.; Osikowicz, W.; Tengsted, C.; Jönsson, S. K. M.; Fahlman, M.; Salaneck, W. R. Orbital-Specific Dynamic Charge Transfer from Fe(II)-Tetraphenylporphyrin Molecules to Molybdenum Disulfide Substrates. *Phys. Rev. B: Condens. Matter Mater. Phys.* **2005**, *72*, 035448.
(84) Fohlisch, A.; Feulner, P.; Hennies, F.; Fink, A.; Menzel, D.; Sanchez-Portal, D.; Echenique, P. M.; Wurth, W. Direct Observation of Electron Dynamics in the Attosecond Domain. *Nature* **2005**, *436*, 373−376.
(85) Piancastelli, M. N. Auger Resonant Raman Studies of Atoms and Molecules. *J. Electron Spectrosc. Relat. Phenom.* **2000**, *107*, 1−26.

DOI: 10.1021/acs.jpcc.6b06006
J. Phys. Chem. C 2016, 120, 26736−26746